Ultralow-power cryogenic thermometry based on optical-transition broadening of a two-level system in diamond

Yongliang Chen,[1] Simon White,[1,*] Evgeny A. Ekimov,[2,3] Carlo Bradac,[4] Milos Toth,[1,5] Igor Aharonovich[1,5] and Toan Trong Tran[1,6,*]

1. School of Mathematical and Physical Sciences, University of Technology Sydney, Ultimo, NSW, 2007, Australia

2. Institute for High Pressure Physics, Russian Academy of Sciences, Troitsk, 142190, Russia

3. Lebedev Physics Institute, Russian Academy of Sciences, Moscow 117924, Russia

4. Department of Physics & Astronomy, Trent University, 1600 West Bank Drive, Peterborough, ON, K9L 0G2, Canada

5. ARC Center of Excellence for Transformative Meta-Optical Systems (TMOS), University of Technology Sydney, Ultimo, NSW, 2007, Australia

6. School of Electrical and Data Engineering, University of Technology Sydney, Ultimo, NSW, 2007, Australia

*Corresponding author: simon.white@uts.edu.au

*Corresponding author: trongtoan.tran@uts.edu.au

ABSTRACT

Cryogenic temperatures are the prerequisite for many advanced scientific applications and technologies. The accurate determination of temperature in this range and at the sub-micrometer scale is, however, non-trivial. This is due to the fact that temperature reading in cryogenic conditions can be inaccurate due to optically-induced heating. Here, we present an ultralow-power, optical thermometry technique that operates at cryogenic temperatures. The technique exploits the temperature-dependent linewidth broadening measured by resonant photoluminescence of a two-level system—a germanium-vacancy color center in a nanodiamond host. The proposed technique achieves a relative sensitivity of ~20% K^{-1}, at 5 K. This is higher than any other all-optical nanothermometry method. Additionally, it achieves such sensitivities while employing excitation powers of just a few tens of nanowatts—several orders of magnitude lower than other traditional optical thermometry protocols. To showcase the performance of the method, we demonstrate its ability to accurately read out local differences in temperatures at various target locations of a custom-made microcircuit. Our work

is a definite step towards the advancement of nanoscale optical thermometry at cryogenic temperatures.

KEYWORDS: nanothermometers, photoluminescence excitation, cryogenic thermometry, germanium-vacancy, nanodiamonds, resonant excitation.

INTRODUCTION

Cryogenic temperatures—ranging from absolute zero to 120 K—present a crucial window for the exploration of cutting-edge applications, both fundamental and practical, that rely on low temperature operating conditions.[1-3] Advanced realizations, for example in optoelectronics, comprise the recent realization of unconventional superconductivity in misaligned bilayer graphene,[4] the observation of quantum Hall effect in graphene [5] and the demonstration of atomically-thin quantum light-emitting diodes[6] to name a few. To facilitate the rapid advancement of this field, appropriate nanoscale thermometers are required to monitor and determine the local temperatures of these devices with accuracy. To this end, contact-based thermometers such as micro-thermocouples, microresistor probes or scanning thermal microscopes have traditionally been employed.[7-9] These contact-based thermometers, however, display complex probe-sample heat transfer mechanisms that are difficult to model or account for as the samples reach the sub-micrometer scale. Optical thermometry eliminates this problem by employing fluorescent nanoprobes of negligible thermal load as the sensing elements. Among optical nanothermometers, those based on photoluminescent nitrogen-vacancy (NV) and group IV color centers in diamond stand out due to a series of desirable properties.[10] These defects generate photons at various wavelengths and show temperature-controlled spin and spectral characteristics that enables simultaneous, multicolor imaging, and temperature sensing. The defects are also stable over several hundreds of degrees Kelvin and the diamond nanohosts are nontoxic and easy to functionalize to specific environments or moieties. However, they are not free of limitations. Thermometers using diamond nitrogen-vacancy and group IV color centers showcase superior sensitivity at room temperature and beyond,[11] yet their capabilities decrease for temperatures under ~100 K owing to a substantial decline in sensitivity.[12, 13]

Lately, a variety of fluorescent thermometers such as lanthanide phosphonate dimer,[14] metal-organic frameworks (MOFs),[15-19] and doped metal oxide phosphors[20] have been established to determine temperatures in cryogenic conditions. Although a few of these thermometers reach sensitivities as high as ~32% K^{-1},[15, 17] they typically are sub-millimeter in size—which prevents their implementation at the nanoscale. Here, we propose a cryogenic thermometer based on the photoluminescence linewidth broadening of a single negatively-charged germanium vacancy (GeV) color center in nanodiamonds, with an excellent sensitivity of ~20% K^{-1}. This is achieved through resonant excitation of the center using ultralow laser powers (~tens of nanowatt)—several orders of magnitudes lower than other competitive methods. Additionally, the technique can reach nanoscale spatial resolutions, since the active sensing elements are

single, atom-like GeV centers that could potentially be hosted in nanodiamonds just a few nanometers in size.[21]

RESULT AND DISCUSSION

The nanothermometers we propose consist of GeV color centers hosted in nanodiamonds that were grown via high-pressure high-temperature (HPHT, c.f. Methods). Briefly, a powder blend of adamantane ($C_{10}H_{16}$) and tetraphenylgermane ($C_{24}H_{20}Ge$) was pressurized into a small tablet and positioned within a titanium container. The container was pressed at high temperature (1800–2000 °C) and high pressure (9 GPa) inside a reaction chamber and cooled under high pressure to room temperature. The obtained nanodiamonds were subsequently distributed in isopropanol alcohol (IPA), casted on a decontaminated silicon substrate and left to dehydrate on a temperature-controlled hotplate at 60 °C to thoroughly eliminate the remaining solvent.[22] **Figure S1a** in the Supporting information shows the sizes of the nanodiamonds ranging from one hundred to a few hundreds of nanometres. A representative Raman spectrum (**Figure S1b**) collected from a randomly chosen nanodiamond reveals the sharp diamond characteristic peak at ~ 1329 cm^{-1}, indicating that the nanodiamonds are highly crystalline.[22]

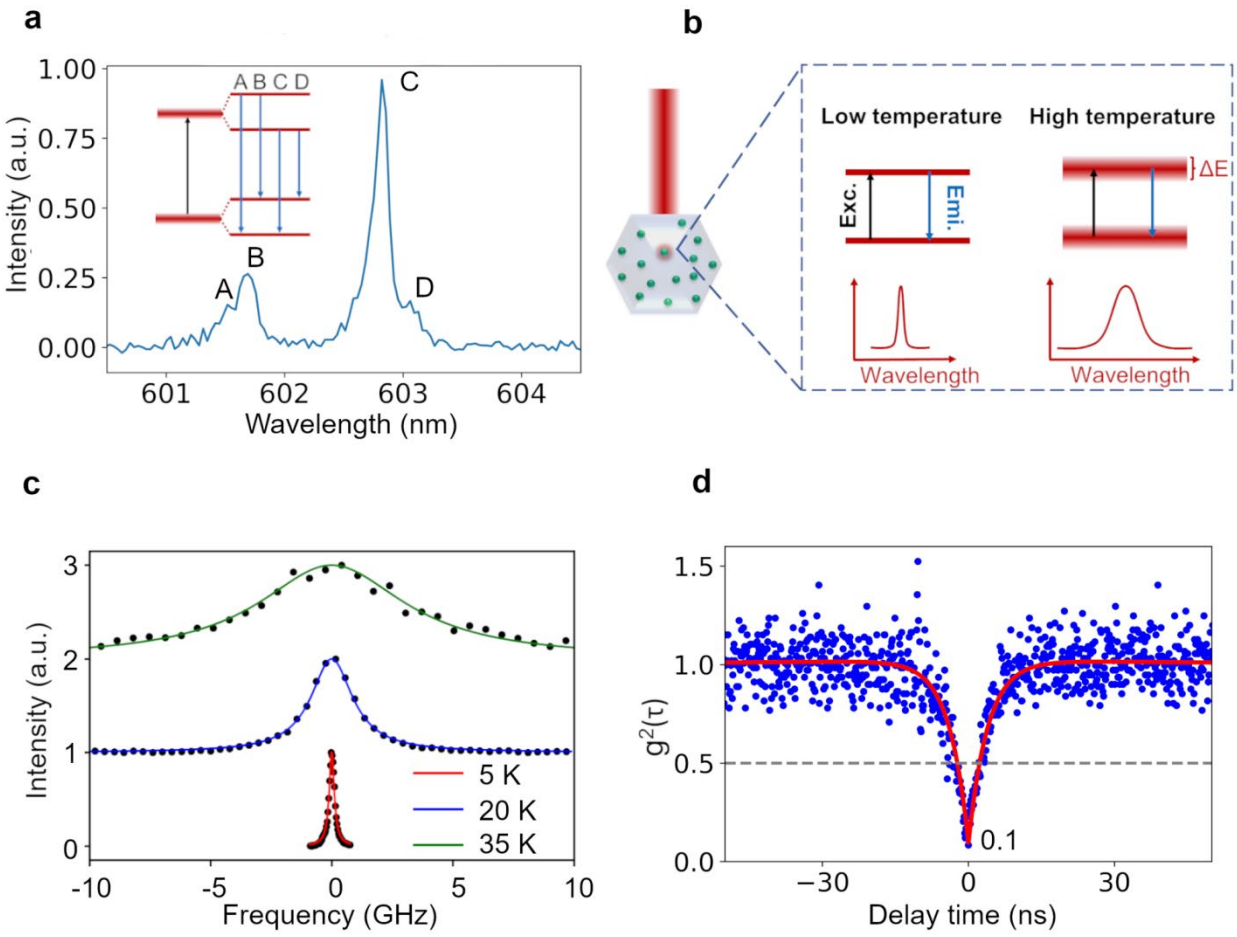

Figure 1. *Emission from an individual GeV color center in a nanodiamond at cryogenic temperatures. a) A representative spectrum acquired by a spectrometer with a grating of 1800 g/mm under the off-resonance excitation of a 532-nm, 300-μW laser at 5 K. Inset: schematic*

depicting the manifold level system of a GeV color center. b) Schematic depicting linewidth broadening due to phonon-mediated coupling. c) Three representative PLE spectra of transition C were acquired at 15-nW laser excitation power at 5 K (red line), 20 K (blue line) and 35 K (green line), respectively, displaying obvious linewidth broadening of the transition C emission with the temperature. d) Second-order autocorrelation measurement from resonant excitation of the GeV center under 200 nW of laser excitation power. The dip of 0.1 indicates the single-photon characteristic of the emission.

The negatively-charged GeV belongs to the group IV diamond color centers alongside the silicon-vacancy (SiV), tin-vacancy (SnV) and lead-vacancy (PbV) center. These defects consist of an interstitial group IV atom (Si, Ge, Sn or Pb) located within two adjacent missing carbons, in the split-vacancy configuration of D_{3d} symmetry.[23] A representative fluorescence spectrum of an ensemble of GeV color centers taken at room-temperature is shown in **Figure S2**. The spectrum clearly features a sharp zero-phonon line (ZPL) alongside a relatively weak phonon sideband (PSB)**.** Owing to its inversion symmetry, the dipole moment of the GeV color center is unsusceptible to local stray fields of the first order created, e.g., by trapped charges and impurities in the diamond lattice.[23] As a result, its ZPL is spectrally stable, making this color center an ideal choice for our demonstration. Furthermore, the ZPL accounts for ~70% of the total fluorescence of the center,[24] which is desirable for several applications in quantum optics and nanophotonics.[25-28] To characterize the optical response of the GeV centers, we loaded the sample into a commercial closed-cycle helium gas cryo-refrigerator (c.f. Methods) with an optically-accessible window. We used a high numerical aperture objective (0.82 NA) to excite individual nanodiamonds and collect their fluorescence at 5–35 K. To showcase the versatility of our technique, we chose nanodiamonds with ensembles of GeVs rather than single ones. This is because our method is inherently selective and allows for the optical interrogation of a single emitter at a time (see below). **Figure 1a** shows a representative spectrum of an ensemble of GeV centers at 5 K, excited with a 532-nm continuous-wave (CW) laser. The four distinctive peaks indicate the four well-known optical transitions of the GeV center at ~601–603 nm, which are labelled A, B, C and D (**Figure 1a**, inset).[27] Note that in the measurement, each peak shows inhomogeneous broadening due to the presence of several GeV centers in the same nanodiamond.[25] The broadening is however too small to be discriminated by our spectrometer equipped with a 1800 g/mm grating (~0.035 nm resolution).

To spectrally isolate an individual GeV from the other centers in the ensemble, we employ resonant photoluminescence excitation (PLE), which is widely used in quantum optics to interrogate a single atom/molecule at a time.[29, 30] In the nanodiamond, the presence of local strain and electric fields causes the ZPL of each emitter to shift from that of any other center by up to tens of gigahertz. This relatively large energy separation and the absence of spectral diffusion makes it possible to isolate a single GeV's optical transition from any other and monitor it as temperature changes. In this study, we employ a narrow laser with a linewidth of ~200 KHz to scan across the ZPL of a single GeV optical transition and measure its spectral linewidth. The spectral broadening from this transition is determined mainly by two factors, i) the linewidth defined by the Fourier transform of the emitter's lifetime, and ii) the linewidth originating from the pure dephasing of the emitter, due to phonons.[31] The former factor does not show any significant temperature dependence up to 300 K and is treated as a constant in

our fit (see discussion below).[26] The latter, however, is strongly affected by temperature variations and displays both linear and cubic temperature-dependent terms—the combination of which can be determined from the PLE scans.[32] **Figure 1b** summarizes the basic idea of our approach. At low temperatures, the spectral linewidth of a single GeV is relatively narrow; it however broadens significantly at higher temperatures. To demonstrate the change in linewidths as the temperature varies, we carried out the PLE measurements using spectral filtering to reject the reflection of the resonant excitation laser. Specifically, we sweep the frequency of the laser across the ZPL while we collect the fluorescence signals from the phonon sideband (PSB) of the emitter into a single-photon avalanche photodiode (SPADP). Since each emitter has four optical transitions (A, B, C and D in Fig. 1A), we focus on transition C, which is the brightest in intensity. Next, we studied the count rate and linewidths of the emitters as a function of excitation power (**Figure S3**). The excitation power was chosen to be 15 nW for all our measurements, unless otherwise specified, since a high signal-to-noise ratio and negligible power-induced broadening are achieved simultaneously at this power.

Figure 1c shows the ZPL lineshape of transition C from a representative GeV color center taken at an excitation power of 15 nW and at various temperatures: 5 K (bottom), 20 K (middle) and 35 K (top). We emphasize that the excitation power we used in this measurement is the lowest across any of the existing all-optical nanothermometry techniques. The low excitation power is key to obtain an accurate readout of the temperature as it eliminates the issue of power-induced heating caused by laser excitation. The absence of spectral diffusion—which would result in the lineshape of the transition to be Gaussian—allows us to fit these peaks with single Lorentzian functions.[32] The measured linewidths are: 231 MHz at 5 K, 2081 MHz at 20 K, and 7380 MHz at 35 K—which corresponds to a 32-fold relative change over the temperature range 5–35 K. Such a strong temperature dependence makes monitoring the linewidth of a single GeV photoemission, via PLE, an excellent strategy for nanoscale thermometry. To verify the quantum emission from the target GeV, we performed a second-order autocorrelation measurement. We set the laser excitation wavelength to be resonant to that of the center's ZPL and recorded the photoluminescence signals from the phonon sideband (PSB) of the emitter. Photon correlations were measured using two single-photon avalanche photodiodes in a Hanbury-Brown and Twiss configuration connected to a high-resolution time tagger (cf. Methods). The strong photon antibunching dip of ~0.1 at zero-delay time in the autocorrelation measurement in **Figure 1d** confirms the emitter to be a single-photon source.

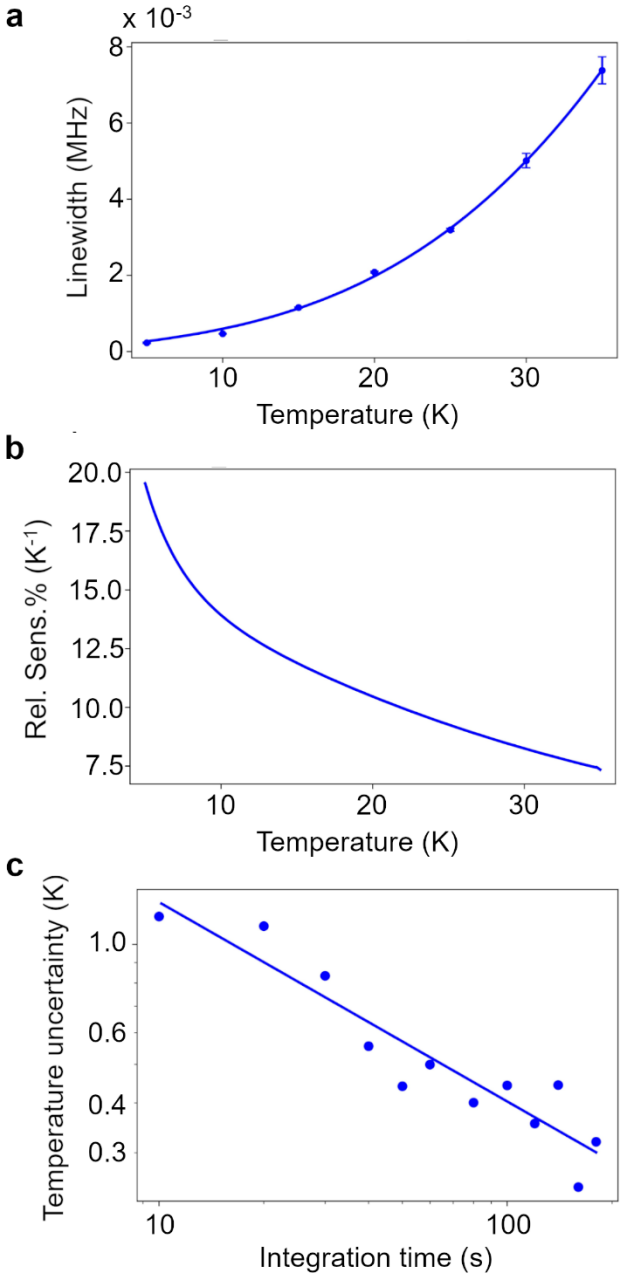

Figure 2. *Characterization of the nanothermometer based on the linewidth broadening of transition C from a single GeV center. a) Temperature dependence of linewidth from the same single transition line in the nanodiamond. Each linewidth is extracted from the Lorentzian fit of the corresponding PLE spectrum. The PLE spectra are acquired with a scanning time of 180 s under a 15-nW laser. The blue line is fitted with the function* $\gamma_{□□□} = □ + □□ + □□^3$. *b) Relative sensitivity of the thermometer as a function of temperature. c) Temperature uncertainty (*σ_T*) of the thermometer plotted against the scanning time (*t_m*) at 5 K. A temperature resolution of 4* $K \cdot Hz^{-1/2}$ *is extracted from the equation fit of* $\eta_{□} = □_{□}\sqrt{□_{□}}$.

We now turn our attention to the calibration of the nanothermometer. To establish the temperature response of the thermometer, we extract the linewidths from the PLE scans across

the transition C of the emitter while increasing the temperature in steps of 5 K, from 5 to 35 K. **Figure 2a** suggests that as the temperature rises, the linewidth of the ZPL increases non-linearly. As mentioned earlier, the temperature dependence of the linewidth is due to two factors and three main components[33]: i) γ_{lt} , the constant linewidth associated to the temperature-invariant lifetime of the emitter, iia) γ_{1st} , a linear temperature-dependent contribution to the linewidth of the first-order, and iib) γ_{2nd} , a cubic temperature-dependent addition to the width due to the second-order electron–phonon interactions with E-symmetric phonon modes.[32] The fitting equation is thus: $\gamma_{□□□} = □_{□□} + □_{1□□} + □_{2□□} = □ + □□ + □□^3$, where $\gamma_{□□□}$ is the total linewidth, c is a constant, while b and a are the coefficients of the second and third components in the equation, respectively. To determine the constant c, we first extracted the lifetime of the emitter from the second-order autocorrelation function in **Figure 1d**, which gave a value of 3.9 ns. The constant c was estimated to be 41 MHz given that: $c = \gamma_{□□} = \frac{1}{2□□}$, where τ is the emitter's lifetime. The experimental data was then fitted to the equation for $\gamma_{□□□}$. The fit was used as the temperature calibration curve for the thermometer. **Figure 2b** displays a graph of the relative sensitivity versus temperature. The relative sensitivity is a key performance metric commonly used in nanothermometry and is defined as $□_□ = \frac{1}{□_{□□□}} \frac{□□_{□□□}}{□□}$. The relative sensitivity of our technique is 20% K^{-1} at 5 K—the highest reported value among all-optical nanothermometry methods. Note that while there are alternative techniques with higher relative sensitivity, ~31%[17] and ~32%[15], they operate at size regimes larger than the nanoscale.

Another important performance index of a thermometer is its temperature resolution. It must be noted that temperature resolution, η_T , is—unlike sensitivity—a relative quantity that can be improved by various means. These include, e.g., increasing the excitation power and/or the integration time, improving the collection efficiency of the optical setup, etc. Specifically, the temperature resolution relates to the integration time t_m and the standard resolution of the measurement, σ_T , via the following expression $\eta_□ = □_□\sqrt{□_□}$. By varying the laser scanning time in the PLE measurement and estimating the standard deviation for the linewidth $\gamma_{□□□}$, we can extract the uncertainty of the temperature readout. **Figure 2c** reveals this correlation with a fit function $\frac{1}{\sqrt{□_□}}$, where t_{m} is the laser scanning time or the integration time. The fit agrees well with our experimental results, showing a temperature resolution η_T =4 $K \cdot Hz^{-1/2}$. This value is relatively modest compared to other all-optical nanothermometers. This follows from the fact that we only excite a single center for a relatively short time, rather than an ensemble of several emitters. However, and importantly, the excitation power we used in this study is only ~tens of nanowatt—several orders of magnitude smaller than other methods. We can objectively take both factors into consideration by estimating the temperature resolution relative to power. This is comparatively high for our technique, of ~6.2 $K \cdot Hz^{-1/2} \cdot W \cdot cm^{-2}$, more than three orders of magnitude greater than that of the next best nanothermometer (1.4×10^4 $K \cdot Hz^{-1/2} \cdot W \cdot cm^{-2}$).[34]

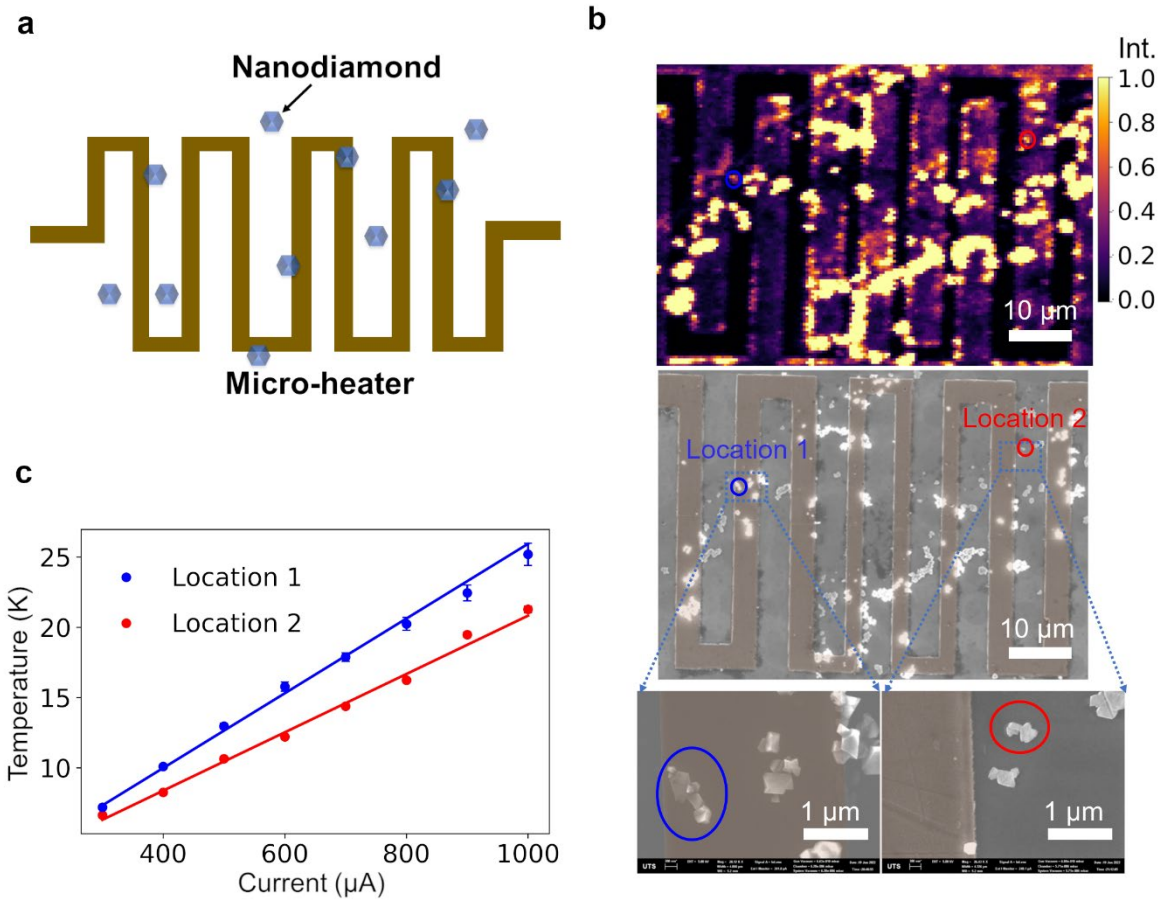

Figure 3. *Temperature monitoring of an operating micro-heater in a cryostat with a fixed temperature of 5 K. a) Schematic illustration of the microcircuit with a nanodiamond thermometer. b) Confocal map and corresponding SEM image of the microcircuit made by EBL. The confocal map is acquired with a 532-nm, 300-μW laser at 5 K. The two circled nanodiamonds are chosen to conduct temperature monitoring. c) Temperature readout of the two selected locations of the operating micro-heater as a function of the applied current. Each temperature readout was calculated from the PLE spectra obtained with a 15-nW laser and a total scanning time of 180 s.*

Finally, we showcase the thermometric capabilities of our thermometer by monitoring the temperature in a few target locations of a microheater. **Figure 3a** displays an illustration of the microheater featuring segments of different widths: six, four and two microns, respectively. We fabricated the microheater using electron-beam lithography (EBL) on a thin layer of chromium (around two-hundred-nanometer thick). The micrometer size of the circuit and its serpentine structure with different widths lead to the circuit displaying different local temperatures across it, depending on the location, when current is modulated through it. The device is therefore an excellent testing ground for illustrating the capability of our thermometer. In the demonstration, the nanodiamonds were drop casted onto the microcircuit; the chip was heated to 60 °C for three minutes and 100 °C for a minute to completely evaporate the remaining solvent and promote strong thermal contact between the nanodiamonds and the microcircuit. To perform the temperature monitoring, we set the sample temperature to 5 K

and varied the input currents to create different local temperatures on the microcircuit by Joule heating. **Figure 3b** (top panel) shows a photoluminescence (PL) confocal map that displays a number of bright spots around or on the microcircuits. A scanning electron microscopy (SEM) image taken from the same area (**Figure 3b**, middle panel) reveals that these bright spots are indeed nanodiamonds. Two selected locations of the nanodiamonds, Location 1 and Location 2, were monitored. **Figure 3b** (bottom panel) shows the close-up images of the two chosen locations in the middle panel—where two clusters of nanodiamonds with size of ~100–500 nm can be discerned. The selection was made to show two representative locations with a different heating response, as nanodiamonds closer to the microcircuit should experience higher temperature variations as current is modulated through the circuit. In each location, we performed PLE measurements on a single GeV and calibrated the center's response to temperature changes, analogously to **Figure 2a**. As we increased the input current by steps of 100 μA, we obtained the corresponding values for the linewidth $\gamma_{\square\square\square}$. We then mapped these values of the linewidth onto the calibration curves and extracted the corresponding temperatures at the two locations. **Figure 3c** shows the local temperature at the two locations plotted against the input current. We note that there seems to be a linear relationship between temperature and input current for both locations. This is likely due to the complex interplay between three factors: 1) the non-linear temperature-dependence of the resistivity of chromium[35], 2) the heat exchange, at steady-state, between the microcircuit and the surrounding reservoir[36], 3) Joule heating of the microcircuit[37]. The thermometer in Location 1 experienced consistently higher temperature than that from Location 2, which is consistent with its position on the edge of the microcircuit, rather than in its close proximity. This result shows that monitoring the PLE linewidth of a single GeV can be effectively used for nanoscale thermometry at cryogenic temperatures. While our measurement was performed using GeV centers, the method can be generalized to any emitter in other host materials including diamond,[38] silicon carbide,[39] hexagonal boron nitride,[40] gallium nitride,[41] silicon nitride,[42] aluminium nitride[43] and many others.[23, 44-46] Furthermore, the current operating temperature limit of our thermometer, ~35 K, is purely a technological limitation set by the hardware of our tunable laser rather than a scientific roadblock.

CONCLUSION

To conclude, we have showcased a cryogenic nanothermometry technique founded on determining the temperature-dependent emission linewidth of a single diamond GeV center via its resonant photoluminescence spectrum. Our nanothermometer exhibits a record-high relative sensitivity of 20% K^{-1} among all-optical nanothermometers and requires a relatively much lower laser power (~tens of nanowatts) thanks to the use of resonant excitation. To showcase the performance of our nanothermometers we employed them to accurately read out local differences in temperature from selected locations of a custom-made microcircuit. Our study demonstrates a powerful and versatile technique that allows monitoring the temperature of fundamental phenomena and/or practical devices at cryogenic conditions.

METHODS

Sample preparation

Ge-doped nanodiamonds were manufactured at high pressures and high temperatures in the germanium (0.2 atomic percent) growth configuration. The nanodiamonds were fabricated at a pressure of nine GPa and a temperature of 1500–1600 °C for approximately sixty seconds. In a typical experiment, a powder mix of Adamantane $C_{10}H_{16}$ (300 mg, > 99%, Sigma-Aldrich) and Tetraphenylgermane $C_{24}H_{20}Ge$ (15mg, 96%, Aldrich) were blended in a mortar and pestle, for around 5 min, pressurized into a small tablet (65 mg) and positioned within a titanium capsule (four millimeters in height, six millimeters in diameter, with a 200 micron-thick wall). An O-ring-shaped, high-pressure vessel was used to produce pressure and temperature inside the reaction chamber.[47] After the reaction, the samples were cooled under high pressure to ambient temperature.

The nanodiamonds were distributed in 2-propanol (IPA) at 0.1% (w/w). The nanodiamonds were around 300-500 nm. Five microliters of the solution were cast on a decontaminated piece of silicon substrate (0.5 x 0.5 cm^2) and left to dehydrate on a heated plate at 60 °C to entirely eliminate the remaining solvent. The silicon substrate was then readily available to be used for optical and structural measurements.

Device fabrication

For fabrication of the microheater, a volume of around 0.1 mL of polymethyl methacrylate resist solution (950 PMMA) was spun on the thermal oxide (~300 nm SiO_2) on Si substrate for 1 min at 3000 rpm to get a uniform coating with a thickness of approximately 200 nm. The resist layer was then selectively irradiated by a scanning electron microscope (SEM) (Zeiss Supra 55VP) controlled by the Raith electron beam lithography (EBL) platform to form the desired pattern. The resist pattern was then developed by dipping the substrate in the resist developer (2-propanol (IPA) / a methyl isobutyl ketone (MIBK), (3:1) solution) for half a minute and IPA (acting as the resist stopper) for sixty seconds. The substrate was cleaned with oxygen plasma for ten seconds under fifty sccm oxygen and one hundred watts of power. A thin chromium layer (around 200-nm thick) was sputtered on the fully patterned resist using a home-built plasma-assisted sputtering chamber. The microheater was then obtained by dipping the chip into acetone (99%) to remove the remaining metal deposition and residual resist.

Optical characterization

The silicon chip was fixed on the helium-cooled stage of an Attocube (Attodry800) closed-cycle cryostat, under high vacuum, and cooled to 5 K. Optical characterizations were carried out with a custom-built laser scanning confocal microscope using a vacuum-compatible objective with a high numerical aperture of 0.82, mounted inside the cryostat (also at the same temperature). A wavelength-adjustable dye laser (Sirah Matisse, 2 DS) with a linewidth around 100 kHz was employed for resonant photoluminescence excitation (PLE). For off-resonant excitation, a 532-nm diode-based laser (Laser Quantum, GEM) was used. In a typical PLE experiment, the laser wavelength was swept across the ZPL, and the phonon sideband (PSB) emission from the quantum emitter was spectrally purified using a 600/14 nm bandpass filter (Semrock), fiber-coupled into a single-mode fiber, and measured with a single-photon avalanche photodiode (Excelitas SPCM-AQRH). Photon antibunching measurements were conducted using a fiber-based beam splitter, a pair of single-photon avalanche photodiodes and

a TimeTagger20 (Swabian), and time-resolved experiments were taken using a 40 MHz pulsed 512 nm laser (PiL051X, Advanced Laser Diode Systems) and the TimeTagger20.

ASSOCIATED CONTENT

Data Availability Statement

Data supporting the results shown in this work are not publicly available at this time but may be acquired from the authors upon reasonable requests.

Supporting Information

The Supporting Information is available free of charge at https://pubs.acs.org

Scanning electron microscopy and Raman characterization of the germanium-vacancy color centers in nanodiamonds; representative spectrum of a GeV color center; intensity and emission linewidths as a function of excitation power for the emitter at the two locations on the microheater in the manuscript.

AUTHOR INFORMATION

Corresponding author

Toan Trong Tran - School of Mathematical and Physical Sciences, University of Technology Sydney, Ultimo, NSW, 2007, Australia; School of Electrical and Data Engineering, University of Technology Sydney, Ultimo, NSW, 2007, Australia; orcid.org/0000-0001-8960-0253; Email: trongtoan.tran@uts.edu.au

Simon White - School of Mathematical and Physical Sciences, University of Technology Sydney, Ultimo, NSW, 2007, Australia; orcid.org/0000-0001-9270-7393; Email: simon.white@uts.edu.au

Author

Yongliang Chen - School of Mathematical and Physical Sciences, University of Technology Sydney, Ultimo, NSW, 2007, Australia; orcid.org/ 0000-0002-2367-8522

Evgeny A. Ekimov - Institute for High Pressure Physics, Russian Academy of Sciences, Troitsk 108840, Moscow, Russia; Lebedev Physics Institute, Russian Academy of Sciences, Moscow 117924, Russia; orcid.org/0000-0001-7644-0078

Carlo Bradac - Trent University, Department of Physics & Astronomy, 1600 West Bank Drive, Peterborough, ON, K9L 0G2; orcid.org/0000-0002-6673-7238

Milos Toth - School of Mathematical and Physical Sciences, University of Technology Sydney, Ultimo, NSW, 2007, Australia; and ARC Center of Excellence for Transformative Meta-Optical Systems (TMOS), Faculty of Science, University of Technology Sydney, Ultimo, NSW, 2007, Australia; orcid.org/0000-0003-1564-4899

Igor Aharonovich - School of Mathematical and Physical Sciences, University of Technology Sydney, Ultimo, NSW, 2007, Australia; and ARC Center of Excellence for Transformative Meta-Optical Systems (TMOS), Faculty of Science, University of Technology Sydney, Ultimo, NSW, 2007, Australia; orcid.org/0000-0003-4304-3935

Author contribution

T. T. T conceptualized the project. Y. C. made the microheater and samples. S. W. and Y. C. conducted the optical characterization and the optical thermometry experiments. Y. C., S. W. and T. T. T analyzed the data. S. W. assembled the optical system and its software. E. E. synthesized the germanium-doped nanodiamonds. T. T. T and S.W. supervised the project. All authors discussed the results, contributed to the data analysis and wrote manuscript.

Funding Sources

T. T. T., I. A. and M. T. thank the Australian Research Council (DE220100487, CE200100010, DP190101058) and the Office of Naval Research Global (N62909-22-1-2028) for financial support. The authors acknowledge the assistance of UTS node of Optofab ANFF with the sample fabrication. C Bradac acknowledges NSERC (RGPIN-2021-03059 and DGECR-2021-00234) and CFI JELF (#41173) for financial support. E.A. Ekimov acknowledges the financial support from the Russian Science Foundation, Grant No. 19-12-00407.

Acknowledgement

The authors acknowledge the ANFF (UTS node) for the use of the diamond reactor facilities.

Notes

The authors declare no competing financial interest.

References

(1) Uppu, R.; Midolo, L.; Zhou, X.; Carolan, J.; Lodahl, P., Quantum-dot-based deterministic photon–emitter interfaces for scalable photonic quantum technology. *Nat. Nanotechnol.* **2021,** *16* (12), 1308-1317.
(2) Liu, Y.; Duan, X.; Shin, H.-J.; Park, S.; Huang, Y.; Duan, X., Promises and prospects of two-dimensional transistors. *Nature* **2021,** *591* (7848), 43-53.
(3) Toth, M.; Aharonovich, I., Single Photon Sources in Atomically Thin Materials. *Annu. Rev. Phys. Chem.* **2019,** *70* (1), 123-142.
(4) Cao, Y.; Fatemi, V.; Fang, S.; Watanabe, K.; Taniguchi, T.; Kaxiras, E.; Jarillo-Herrero, P., Unconventional superconductivity in magic-angle graphene superlattices. *Nature* **2018,** *556* (7699), 43-50.

(5) Zhang, Y.; Tan, Y.-W.; Stormer, H. L.; Kim, P., Experimental observation of the quantum Hall effect and Berry's phase in graphene. *Nature* **2005,** *438* (7065), 201-204.
(6) Palacios-Berraquero, C.; Barbone, M.; Kara, D. M.; Chen, X.; Goykhman, I.; Yoon, D.; Ott, A. K.; Beitner, J.; Watanabe, K.; Taniguchi, T.; Ferrari, A. C.; Atatüre, M., Atomically thin quantum light-emitting diodes. *Nat. Commun.* **2016,** *7* (1), 12978.
(7) Menges, F.; Mensch, P.; Schmid, H.; Riel, H.; Stemmer, A.; Gotsmann, B., Temperature mapping of operating nanoscale devices by scanning probe thermometry. *Nat. Commun.* **2016,** *7*, 10874.
(8) Shekhawat, G. S.; Ramachandran, S.; Jiryaei Sharahi, H.; Sarkar, S.; Hujsak, K.; Li, Y.; Hagglund, K.; Kim, S.; Aden, G.; Chand, A.; Dravid, V. P., Micromachined Chip Scale Thermal Sensor for Thermal Imaging. *ACS Nano* **2018,** *12* (2), 1760-1767.
(9) Jiang, S.-D.; Liu, J.-Q.; Yang, B.; Zhu, H.-Y.; Yang, C.-S., Microfabrication of thin film temperature sensor for cryogenic measurement. *Microsystem Technologies* **2013,** *20* (3), 451-456.
(10) Bradac, C.; Lim, S. F.; Chang, H.-C.; Aharonovich, I., Optical Nanoscale Thermometry: From Fundamental Mechanisms to Emerging Practical Applications. *Adv. Opt. Mater.* **2020,** *8* (15), 2000183.
(11) Neumann, P.; Jakobi, I.; Dolde, F.; Burk, C.; Reuter, R.; Waldherr, G.; Honert, J.; Wolf, T.; Brunner, A.; Shim, J. H.; Suter, D.; Sumiya, H.; Isoya, J.; Wrachtrup, J., High-Precision Nanoscale Temperature Sensing Using Single Defects in Diamond. *Nano Lett.* **2013,** *13* (6), 2738-2742.
(12) Chen, X.-D.; Dong, C.-H.; Sun, F.-W.; Zou, C.-L.; Cui, J.-M.; Han, Z.-F.; Guo, G.-C., Temperature dependent energy level shifts of nitrogen-vacancy centers in diamond. *Appl. Phys. Lett.* **2011,** *99* (16), 161903.
(13) Tran, T. T.; Regan, B.; Ekimov, E. A.; Mu, Z.; Zhou, Y.; Gao, W.-b.; Narang, P.; Solntsev, A. S.; Toth, M.; Aharonovich, I.; Bradac, C., Anti-Stokes excitation of solid-state quantum emitters for nanoscale thermometry. *Sci. Adv.* **2019,** *5* (5), eaav9180.
(14) Ren, M.; Brites, C. D. S.; Bao, S.-S.; Ferreira, R. A. S.; Zheng, L.-M.; Carlos, L. D., A cryogenic luminescent ratiometric thermometer based on a lanthanide phosphonate dimer. *J. Mater. Chem. C* **2015,** *3* (33), 8480-8484.
(15) D'Vries, R. F.; Álvarez-García, S.; Snejko, N.; Bausá, L. E.; Gutiérrez-Puebla, E.; de Andrés, A.; Monge, M. Á., Multimetal rare earth MOFs for lighting and thermometry: tailoring color and optimal temperature range through enhanced disulfobenzoic triplet phosphorescence. *J. Mater. Chem. C* **2013,** *1* (39), 6316-6324.
(16) Lustig, W. P.; Mukherjee, S.; Rudd, N. D.; Desai, A. V.; Li, J.; Ghosh, S. K., Metal–organic frameworks: functional luminescent and photonic materials for sensing applications. *Chem. Soc. Rev.* **2017,** *46* (11), 3242-3285.
(17) Liu, X.; Akerboom, S.; Jong, M. d.; Mutikainen, I.; Tanase, S.; Meijerink, A.; Bouwman, E., Mixed-Lanthanoid Metal–Organic Framework for Ratiometric Cryogenic Temperature Sensing. *Inorg. Chem.* **2015,** *54* (23), 11323-11329.
(18) Wang, Z.; Ananias, D.; Carné-Sánchez, A.; Brites, C. D. S.; Imaz, I.; Maspoch, D.; Rocha, J.; Carlos, L. D., Lanthanide–Organic Framework Nanothermometers Prepared by Spray-Drying. *Adv. Funct. Mater.* **2015,** *25* (19), 2824-2830.
(19) Cui, Y.; Zou, W.; Song, R.; Yu, J.; Zhang, W.; Yang, Y.; Qian, G., A ratiometric and colorimetric luminescent thermometer over a wide temperature range based on a lanthanide coordination polymer. *Chem. Commun.* **2014,** *50* (6), 719-721.
(20) Jahanbazi, F.; Mao, Y., Recent advances on metal oxide-based luminescence thermometry. *J. Mater. Chem. C* **2021,** *9* (46), 16410-16439.
(21) Vlasov, I. I.; Shiryaev, A. A.; Rendler, T.; Steinert, S.; Lee, S.-Y.; Antonov, D.; Vörös, M.; Jelezko, F.; Fisenko, A. V.; Semjonova, L. F.; Biskupek, J.; Kaiser, U.; Lebedev, O. I.;

Sildos, I.; Hemmer, P. R.; Konov, V. I.; Gali, A.; Wrachtrup, J., Molecular-sized fluorescent nanodiamonds. *Nat. Nanotechnol.* **2014,** *9* (1), 54-58.
(22) Kondrina, K. M.; Kudryavtsev, O. S.; Vlasov, I. I.; Khmelnitskiy, R. A.; Ekimov, E. A., High-pressure synthesis of microdiamonds from polyethylene terephthalate. *Diamond Relat. Mater.* **2018,** *83*, 190-195.
(23) Bradac, C.; Gao, W.; Forneris, J.; Trusheim, M. E.; Aharonovich, I., Quantum nanophotonics with group IV defects in diamond. *Nat. Commun.* **2019,** *10* (1), 5625.
(24) Palyanov, Y. N.; Kupriyanov, I. N.; Borzdov, Y. M.; Surovtsev, N. V., Germanium: a new catalyst for diamond synthesis and a new optically active impurity in diamond. *Sci. Rep.* **2015,** *5* (1), 14789.
(25) Chen, D.; Fröch, J. E.; Ru, S.; Cai, H.; Wang, N.; Adamo, G.; Scott, J.; Li, F.; Zheludev, N.; Aharonovich, I.; Gao, W., Quantum Interference of Resonance Fluorescence from Germanium-Vacancy Color Centers in Diamond. *Nano Lett.* **2022,** *22* (15), 6306-6312.
(26) Bhaskar, M. K.; Sukachev, D. D.; Sipahigil, A.; Evans, R. E.; Burek, M. J.; Nguyen, C. T.; Rogers, L. J.; Siyushev, P.; Metsch, M. H.; Park, H.; Jelezko, F.; Lončar, M.; Lukin, M. D., Quantum Nonlinear Optics with a Germanium-Vacancy Color Center in a Nanoscale Diamond Waveguide. *Phys. Rev. Lett.* **2017,** *118* (22), 223603.
(27) Siyushev, P.; Metsch, M. H.; Ijaz, A.; Binder, J. M.; Bhaskar, M. K.; Sukachev, D. D.; Sipahigil, A.; Evans, R. E.; Nguyen, C. T.; Lukin, M. D.; Hemmer, P. R.; Palyanov, Y. N.; Kupriyanov, I. N.; Borzdov, Y. M.; Rogers, L. J.; Jelezko, F., Optical and microwave control of germanium-vacancy center spins in diamond. *Phys. Rev. B* **2017,** *96* (8), 081201.
(28) Fan, J.-W.; Cojocaru, I.; Becker, J.; Fedotov, I. V.; Alkahtani, M. H. A.; Alajlan, A.; Blakley, S.; Rezaee, M.; Lyamkina, A.; Palyanov, Y. N.; Borzdov, Y. M.; Yang, Y.-P.; Zheltikov, A.; Hemmer, P.; Akimov, A. V., Germanium-Vacancy Color Center in Diamond as a Temperature Sensor. *ACS Photonics* **2018,** *5* (3), 765-770.
(29) Wrigge, G.; Gerhardt, I.; Hwang, J.; Zumofen, G.; Sandoghdar, V., Efficient coupling of photons to a single molecule and the observation of its resonance fluorescence. *Nat. Phys.* **2008,** *4* (1), 60-66.
(30) Tamarat, P.; Gaebel, T.; Rabeau, J. R.; Khan, M.; Greentree, A. D.; Wilson, H.; Hollenberg, L. C. L.; Prawer, S.; Hemmer, P.; Jelezko, F.; Wrachtrup, J., Stark Shift Control of Single Optical Centers in Diamond. *Phys. Rev. Lett.* **2006,** *97* (8), 083002.
(31) Buckley, S.; Rivoire, K.; Vučković, J., Engineered quantum dot single-photon sources. *Rep. Prog. Phys* **2012,** *75* (12), 126503.
(32) Jahnke, K. D.; Sipahigil, A.; Binder, J. M.; Doherty, M. W.; Metsch, M.; Rogers, L. J.; Manson, N. B.; Lukin, M. D.; Jelezko, F., Electron–phonon processes of the silicon-vacancy centre in diamond. *New J. Phys.* **2015,** *17* (4), 043011.
(33) Donley, E. A.; Bonsma, S.; Palm, V.; Burzomato, V.; Wild, U. P.; Plakhotnik, T., Zero–phonon lines of single molecules in polyethylene down to millikelvin temperatures. *J. Lumin.* **2000,** *87-89*, 109-114.
(34) Chen, Y.; Li, C.; Yang, T.; Ekimov, E. A.; Bradac, C.; Ha, S. T.; Toth, M.; Aharonovich, I.; Tran, T. T. Real-time ratiometric optical nanoscale thermometry. ACS Nano **2023**, Article ASAP. DOI: 10.1021/acsnano.2c10974 (accessed 2023-02-11).
(35) Sawabu, M.; Ohashi, M.; Ohashi, K.; Miyagawa, M.; Kubota, T.; Takanashi, K., The electrical resistivity of epitaxially deposited chromium films. *Journal of Physics: Conference Series* **2017,** *871* (1), 012002.
(36) Pop, E.; Sinha, S.; Goodson, K. E., Heat Generation and Transport in Nanometer-Scale Transistors. *Proceedings of the IEEE* **2006,** *94* (8), 1587-1601.
(37) Mecklenburg, M.; Hubbard, W. A.; White, E. R.; Dhall, R.; Cronin, S. B.; Aloni, S.; Regan, B. C., Nanoscale temperature mapping in operating microelectronic devices. *Science* **2015,** *347* (6222), 629-632.

(38) Doherty, M. W.; Manson, N. B.; Delaney, P.; Jelezko, F.; Wrachtrup, J.; Hollenberg, L. C. L., The nitrogen-vacancy colour centre in diamond. *Phys. Rep.* **2013,** *528* (1), 1-45.
(39) Anderson, C. P.; Glen, E. O.; Zeledon, C.; Bourassa, A.; Jin, Y.; Zhu, Y.; Vorwerk, C.; Crook, A. L.; Abe, H.; Ul-Hassan, J.; Ohshima, T.; Son, N. T.; Galli, G.; Awschalom, D. D., Five-second coherence of a single spin with single-shot readout in silicon carbide. *Sci. Adv.* **2022,** *8* (5), eabm5912.
(40) Tran, T. T.; Bray, K.; Ford, M. J.; Toth, M.; Aharonovich, I., Quantum emission from hexagonal boron nitride monolayers. *Nat. Nanotechnol.* **2016,** *11* (1), 37-41.
(41) Berhane, A. M.; Jeong, K.-Y.; Bodrog, Z.; Fiedler, S.; Schröder, T.; Triviño, N. V.; Palacios, T.; Gali, A.; Toth, M.; Englund, D.; Aharonovich, I., Bright Room-Temperature Single-Photon Emission from Defects in Gallium Nitride. *Adv. Mater.* **2017,** *29* (12), 1605092.
(42) Senichev, A.; Martin, Z. O.; Peana, S.; Sychev, D.; Xu, X.; Lagutchev, A. S.; Boltasseva, A.; Shalaev, V. M., Room-temperature single-photon emitters in silicon nitride. *Sci. Adv.* **2021,** *7* (50), eabj0627.
(43) Bishop, S. G.; Hadden, J. P.; Alzahrani, F. D.; Hekmati, R.; Huffaker, D. L.; Langbein, W. W.; Bennett, A. J., Room-Temperature Quantum Emitter in Aluminum Nitride. *ACS Photonics* **2020,** *7* (7), 1636-1641.
(44) Aharonovich, I.; Englund, D.; Toth, M., Solid-state single-photon emitters. *Nat. Photonics* **2016,** *10* (10), 631-641.
(45) Awschalom, D. D.; Hanson, R.; Wrachtrup, J.; Zhou, B. B., Quantum technologies with optically interfaced solid-state spins. *Nat. Photonics* **2018,** *12* (9), 516-527.
(46) Lohrmann, A.; Johnson, B. C.; McCallum, J. C.; Castelletto, S., A review on single photon sources in silicon carbide. *Rep. Prog. Phys* **2017,** *80* (3), 034502.
(47) Ekimov, E. A.; Lyapin, S. G.; Kondrin, M. V., Tin-vacancy color centers in micro- and polycrystalline diamonds synthesized at high pressures. *Diamond Relat. Mater.* **2018,** *87*, 223-227.

For Table of Contents Use Only

Ultralow-power cryogenic thermometry based on optical-transition broadening of a two-level system in diamond

Yongliang Chen,[1] Simon White,[1,*] Evgeny A. Ekimov,[2,3] Carlo Bradac,[4] Milos Toth,[1,5] Igor Aharonovich[1,5] and Toan Trong Tran[1,6,*]

The broadening of a single optical transition in germanium-vacancy center in nanodiamonds is used as an ultra-low-powered cryogenic nanothermometer. The nanothermometers are used to sense local temperatures on a Joule-heating microheater.